THE JOURNAL OF PHYSICAL CHEMISTRY C

pubs.acs.org/JPCC Article

Combined Impact of Denticity and Orientation on Molecular-Scale Charge Transport

Published as part of The Journal of Physical Chemistry virtual special issue "David N. Beratan Festschrift".

Parisa Yasini, Stuart Shepard, Tim Albrecht, Manuel Smeu,* and Eric Borguet*

Cite This: *J. Phys. Chem. C* 2020, 124, 9460–9469 Read Online

ABSTRACT: Reducing the dimensions of electronic devices to the nanoscale is an important objective with significant scientific and technical challenges. In molecule-based approaches, the orientation of the molecule and coordination to electrodes (denticity) can dramatically affect the electrical properties of the junction. Typically, higher conductance is associated with shorter transport distances and stronger molecule–electrode coupling; however, this is not always the case, as highlighted in this study. We focused on 7,7,8,8-tetracyanoquinodimethane (TCNQ) and 2,3,5,6-tetrafluoro-7,7,8,8-tetracyanoquinodimethane (F_4TCNQ) molecules and have used the scanning tunneling microscopy break junction (STM-BJ) method to measure the electrical conductance of single molecules bridged between gold electrodes with different molecular orientations and with varying denticities. In conjunction with the experiments, density functional theory (DFT) and nonequilibrium Green's function (NEGF) calculations were performed to determine the conductance of four distinct molecular configurations. The calculated conductances show how different configurations and denticities influence the molecular orbital offsets with respect to the Fermi level and provide assignments for the experimental results. Surprisingly, lower denticity results in higher conductance, with the highest predicted molecular conductance being 0.6 G_0, which is explained by the influence of molecule–electrode coupling on the energy of molecular orbitals relative to the Fermi level. These results highlight the importance of molecular geometry and binding configuration of the molecule to the electrode. Consequently, our findings have profound ramifications for applications in which orbital alignment is critical to the efficiency of charge transport, such as in dye sensitized solar cells, molecular switches, and sensors.

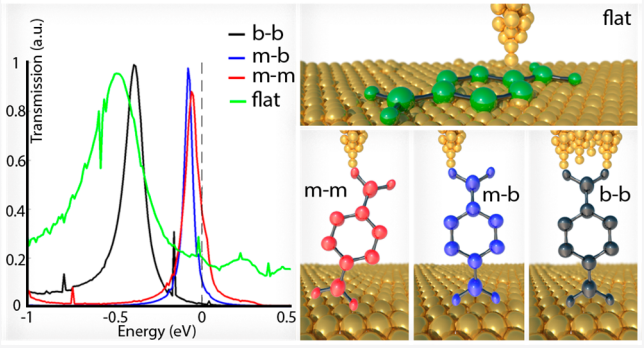

INTRODUCTION

Achieving detailed insight into interfacial charge transport through single-molecule junctions is an integral step toward the practical application of molecular devices, e.g., solar cells, photocatalysts, and organic–inorganic/nanoparticle hybrid systems.[1,2] Recently, researchers have focused on modulation of the Fermi level alignment relative to HOMO/LUMO and the metal–molecule coupling using external stimuli, e.g., environmental pH, conformational change, applied potential, and light.[3−8] For example, studies have employed the electrochemical potential by incorporating a third (gate) electrode to tune the Fermi level of the electrodes relative to the energy level of molecular orbitals.[9−18] While it is known that the geometry of the molecule in the junction can remarkably influence charge transport through a single molecule,[19] there has been little effort to use denticity and binding contact between a molecule and a metal as a control parameter to manipulate charge transport across the junction.[20]

In this contribution, we take advantage of the fact that applying a potential to the substrate can induce a change in the adsorbate–substrate interaction, including denticity and binding contact, by altering the geometry of the molecule on the surface and hence in the measured single-molecule conductance (SMC).[21] For example, using an electrified substrate one can drive the formation of highly ordered 2-dimensional assemblies that immobilize the adsorbates flat on the surface, facilitating charge transport measurements perpendicular to the molecular plane.[22−24] Here, we focused on 7,7,8,8-tetracyanoquinodimethane (TCNQ) and 2,3,5,6-tetrafluoro-7,7,8,8-tetracyanoquinodimethane (F_4TCNQ) which are

Received: November 11, 2019
Revised: March 19, 2020
Published: April 17, 2020

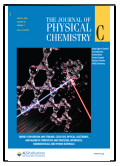

https://dx.doi.org/10.1021/acs.jpcc.9b10566
J. Phys. Chem. C 2020, 124, 9460–9469

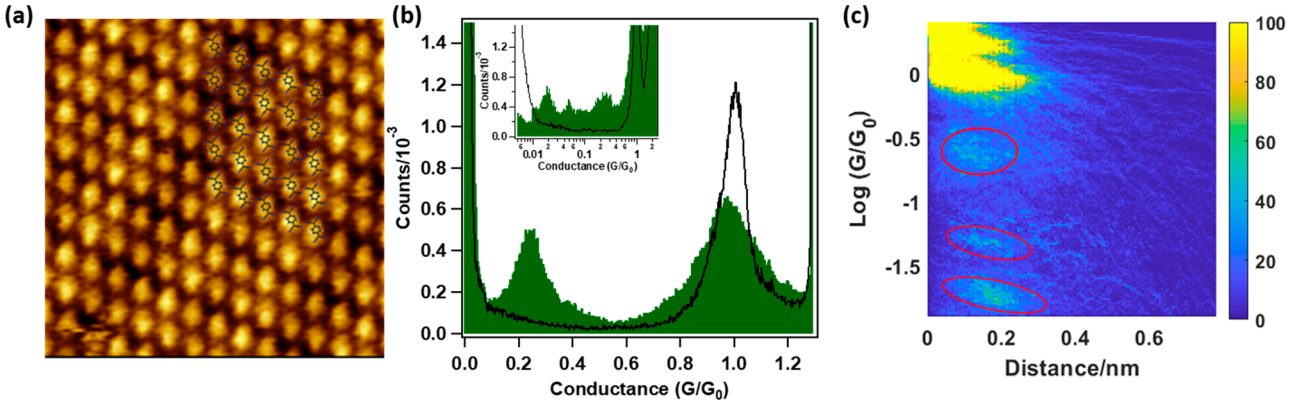

Figure 1. (a) STM image of TCNQ/0.05 M H_2SO_4 on Au(111) at V_S = 0 V_{SCE}, V_{bias} = 0.03 V, and I_t = 0.1 nA, with scan area 10 × 10 nm^2. (b) Conductance histograms for TCNQ recorded in 0.05 M H_2SO_4 at V_S = 0 V_{SCE} (green, generated using 3226 current-distance curves) and V_S = 0.7 V_{SCE} (black line, generated using 3163 current-distance curves) at V_{bias}= 0.1 V. The inset is the log binned conductance histogram recorded at V_S = 0 V_{SCE} (green, generated using 3360 current-distance curves) and V_S = 0.7 V_{SCE} (black line, generated using 1926 current-distance curves) at V_{bias} = 0.05 V. (c) 2D histogram generated from data recorded at V_S = 0 V_{SCE}. All histograms are generated without data selection.

widely used in the formation of charge transfer complexes.[25−28] The intriguing physical characteristics, e.g., magnetic, optical, and electrical properties,[29−33] of these electron acceptors make metal−TCNQ/F_4TCNQ junctions promising candidates for electronic device components such as sensors, memories, and data storage applications.[34,35] Recently, surface science techniques, e.g., scanning tunnelling microscopy (STM), atomic force microscopy (AFM), and scanning tunnelling spectroscopy (STS), have been used to determine the structure and the electronic properties of self-assembled monolayers of TCNQ on Au(111),[29] on Ag(111) and Ag(100),[32,36,37] and Cu(111)[38] in ultrahigh vacuum (UHV), as well as on Au(111)[39] and Cu(111)[40] in an electrochemical environment. Furthermore, the geometry and electronic structure of F_4TCNQ molecular networks on Au(111)[41,42] and on Cu(100)[43] have been investigated under UHV. Reversible modulation of the charge state of isolated F_4TCNQ using back-gated graphene devices has been studied using high resolution noncontact AFM and STM under UHV at low temperature.[44] In a recent STM-BJ experiment, the conductance of a molecular wire (π-extended tetrathiafulvalene) has been measured upon the formation of a charge transfer complex with F_4TCNQ molecules.[45] However, to the best of our knowledge, the conductance values for single TCNQ and F_4TCNQ molecules and the effect of molecule−electrode denticity have not been reported.

Here, using the combination of STM and break junction (BJ) methods, we studied the structure and charge transport properties of TCNQ and F_4TCNQ on a Au(111) electrode in an electrochemical environment. Our results indicate that TCNQ and F_4TCNQ exhibit distinct orientation and denticity dependent conductance states which could ultimately be exploited toward the design of electromechanical single molecule switches and other nanoscale electronics. Moreover, our NEGF-DFT electron transport calculations predict a conduction pathway of 0.6 G_0 for a low denticity (mono-mono) TCNQ configuration. This unusually large conductance is shown to arise from the interplay between denticity and favorable alignment of the frontier orbital of the molecule with the Fermi level of the electrodes.

RESULTS AND DISCUSSION

In Situ STM and SMC of TCNQ on Au(111). The STM images show that, after addition of 0.1 mL of saturated TCNQ solution in 0.05 M sulfuric acid to the STM cell at potentials more negative than the point of zero charge (PZC) of bare Au(111) in sulfuric acid, a long-range ordered molecular structure extending for hundreds of nanometers over the surface was formed on the electrode. The existence of the underlying herringbone reconstruction, confirmed with STM images and cyclic voltammetry (CV) (Figure S1), suggests physisorption and a weak interaction of the ordered layer of TCNQ with the Au surface. Detailed inspection and cross-section analysis of the STM images revealed that the individual TCNQ molecules lie flat on the negatively charged Au(111) electrode (Figure 1a and Figure S2). We propose a structural model with one molecule per unit cell and hypothesize that this geometry is due to four possible hydrogen bonds (red dashed lines, Figure S2c) per molecule between the CN groups and H atoms of neighboring molecules. Further details are provided in the Supporting Information.

An STM study showed ordered structure formation of TCNQ on the Au(111) surface induced by molecule−surface interactions at the potential of 0.27 V_{SCE}.[39] The resulting ordered structure contains two molecules per unit cell.[39] However, at a potential of −0.22 V_{SCE}, due to weaker interactions of the phenyl ring with Au(111) and the formation of intermolecular hydrogen bonds, a different ordered structure is observed with six molecules per unit cell.[39] UHV-STM investigations revealed an ordered structure at 5 K in which all terminal N and H atoms are involved in intramolecular interactions.[29]

As the surface potential is swept more positive, an order-to-disorder transition starts gradually until complete disorder is achieved at the surface potential of 0.5 V_{SCE} (Figure S3). This transition is consistent with the cyclic voltammetry peaks observed at 0.50−0.65 V_{SCE} (Figure S1). When the potential is swept back to its original values (negatively charged Au surface), the TCNQ molecules start to reappear until the complete formation of the ordered layer consistent with the reversibility of the order-to-disorder transition of TCNQ on Au(111)[46] (Figure S3).

Following the STM imaging, we conducted single-molecule conductance measurements on TCNQ at electrode potentials

https://dx.doi.org/10.1021/acs.jpcc.9b10566
J. Phys. Chem. C 2020, 124, 9460−9469

above and below the phase transition (presumably negatively and positively charged electrodes). In the STM break junction method, the STM tip is gradually brought to the Au(111) surface to form a gentle contact with the surface and then withdrawn to form a nanogap between the gold tip and the gold surface (Figure S6). More than 3000 current−distance traces were recorded at the surface potential of 0 V_{SCE} to generate 1D and 2D conductance histograms (Figure 1b,c) showing two well-defined peaks in the linear histogram at 0.22 and 1.00 G_0 corresponding to molecular and atomic gold junctions, respectively.

The assignment of the 0.22 G_0 peak to a molecular junction is correlated with the existence of the ordered adsorbate structure, facilitating the direct π binding of the TCNQ ring to the electrode and increasing the probability of the formation of Au−TCNQ−Au junctions with quasi-flat oriented TCNQ.[24] STM images of ordered molecular structures before and after the break junction procedure (reported in our previous studies) show the formation of local holes/islands with the size of one or a few molecules while the surrounding ordered molecular network remained intact.[22,23] The junction formation is a gentle and soft process (the tip moves toward the surface in 0.1 nm steps until it touches the surface and does not go far beyond the initial contact).[22,23] High resolution STM images taken after break junction measurements with the same tip strongly indicate that the tip does not undergo a destructive crashing and deformation during break junction formation. In addition, after reviewing many individual current−distance curves, we noticed that, among the traces showing atomic/molecular features, ∼50% of the traces that contain molecular features do not show gold atom plateaus (Figure S7). Hence, this suggests that for half of the measured traces, the tip did not form a gold−gold junction and likely did not disturb the ordered structure.[22,23] Therefore, our proposed scenario is that the molecule trapped between the tip and the Au(111), whose geometry is stabilized through the formation of a two-dimensional monolayer, could remain quasi-flat, giving rise to the high conductance value. Upon further elongation, the tip can lift the trapped molecule from the surface through one or more of its anchoring groups, and further retraction could result in removing the molecule from the surface.

The observation of high conductance is consistent with previous SMC measurements and calculations on small benzene derivatives showing that measuring the conductance perpendicular to the benzene ring results in high conductance values compared to measurements along the molecular plane due to the direct π interaction of the benzene ring with the metal surface.[22−24,47−50] Therefore, we attribute the 0.22 G_0 conductance peak to charge transport perpendicular to the central ring of molecules immobilized on the Au(111) surface through the intermolecular hydrogen bonding between neighboring molecules. It is worth mentioning that the details of the metal−molecule−metal junction geometry, and its structural evolution during the tip retraction step, are still not well-understood and need further experimental and theoretical investigation. Therefore, the proposed model for the flat oriented molecule is a simplified picture, and the initial geometry in the junction could deviate from the ideal flat configuration. The flat model is discussed to differentiate between two states: when the tip forms a contact with the π-system of the molecule and when it is anchored to one of the functional groups.

A detailed inspection of the 1D histogram created at the negatively charged gold surface (Figure 1b, inset with log scale plotting) shows two peaks at 0.02 and 0.05 G_0. Considering the fact that TCNQ molecules lie quasi-flat at this potential, and that the nitrile is a reliable and stable anchoring group to form single-molecule junctions,[51−54] we attribute these two lower conductance values to two possible tip-induced geometries of the molecule in the junction formed by bidentate−bidentate (b−b) and monodentate−bidentate (m−b) molecular binding to the tip via nitrile groups, respectively (geometries are provided in Figure 4 and will be discussed in detail). This hypothesis is supported by density functional theory modeling which shows similar low conductance values for these configurations (*vide infra*), likely induced by pulling the molecule up from the surface. In this fashion, after formation of a high conductance junction with a quasi-flat-lying molecule, the tip can overcome the relatively weak metal−π interaction and lift the molecule off the surface through anchoring of CN groups to the gold tip while it retracts from the surface.[55] This gives rise to b−b and m−b configurations as the junction elongates. Previous experimental and theoretical studies have shown that charge transport along the molecular plane (upright geometry) of benzene derivatives exhibits conductance values close to 10^{-2} G_0.[56−63] The histogram constructed from the current−distance traces measured at 0.70 V_{SCE} (Figure 1b, black line) in the high current range does not show a well-defined peak in the 1000−2000 nA current region, suggesting that high conductivity junctions (flat orientation) are not formed at this potential. This is likely due to the lack of ordered molecular structures suggesting a random, nonplanar orientation of the molecules on the positively charged surface as observed in the STM images (Figure S3). Previously, we showed that, in a series of STM-BJ experiments performed on benzene derivatives (benzene, toluene, and 1,2,4-trichlorobenzene), the lack of long-range ordered molecular structures diminishes the probability of the formation of junctions with the aromatic ring perpendicular to the STM tip.[24] Accordingly, the probability of junction formation with the molecular plane perpendicular to the tip and the surface (quasi-flat orientation) at the positive potential decreases significantly.

In order to provide a more complete analysis including a different range of geometries, we investigated the conductance characteristics of TCNQ molecules in a lower current region while they are adsorbed on the positively charged electrode surface, presumably disordered. The all-data current histogram constructed from current−distance curves measured at a positively charged gold surface in the lower current region (using a 10 nA/V preamplifier) shows no peak (Figure 2, black line). However, individual current−distance curves show long steps (∼1 nm) with different conductance values (Figure 2, inset). As the histogram based analysis focuses on the most probable events in single-molecule junction measurement, less frequent occurrences might be masked by the background noise or a wider distribution of values. The lack of a well-defined peak in the conductance histogram at the positively charged surface could reflect the existence of several different, low probability, molecular binding configurations and different current values associated with them.[20]

This observation leads us to manually sort the current−distance curves and to categorize them on the basis of current step values for subsequent analysis (further details are provided in the Supporting Information (section 4b)). The constructed

https://dx.doi.org/10.1021/acs.jpcc.9b10566
J. Phys. Chem. C 2020, 124, 9460−9469

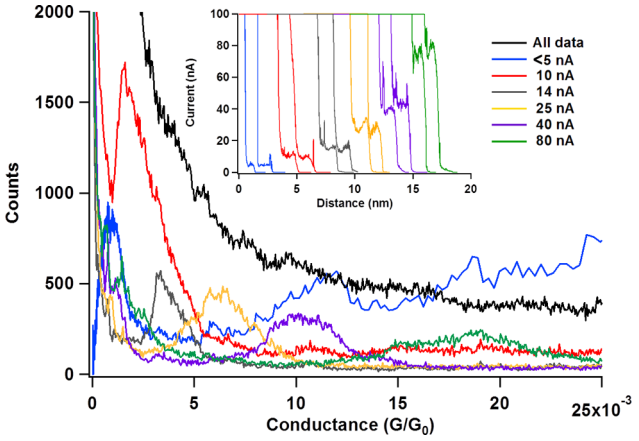

Figure 2. Histograms of all data (~8500 curves, black line) and with selected curves with the step values: below 5 nA (~16% of all curves, blue), 5−10 nA (~18% of all curves, red), 10−20 nA (~7% of all curves, gray), 20−30 nA (~6% of all curves, yellow), 30−50 nA (~4% of all curves, purple), 50−90 nA (~3% of all curves, green). Inset: Typical current−distance curves of TCNQ recorded in 0.05 M H_2SO_4 at V_{bias} = 0.05 V, V_S = 0.7 V_{SCE} categorized based on current values.

1D histograms with selected curves show several peaks with different values (Figure 2). On the basis of the STM images, TCNQ molecules do not form ordered structures at the positively charged Au(111) surface, and they might be randomly adsorbed on the surface in different orientations. Of the detected conductance values, the 0.02 G_0 peak is consistent with the peak observed in the conductance histogram collected at the negatively charged gold surface, which we attributed to a tip-lifted upright molecular geometry.

As a conventional histogram approach with all data failed to pick out the selected events in the data set and to further consolidate our analysis of the low conductance region, we employed the multiparameter vector classification (MPVC) approach.[64] The MPVC analysis results show the emergence of molecular features when the target molecules are present but did not reveal distinct and well-defined groups of current−distance traces (in terms of their overall shape). Nonetheless, the comparative analysis between manual selection and MPVC classification of low conductance data shows apparent correlation between the cluster allocation and the hand-selection (further details are provided in the Supporting Information, Figures S8−S10).

In Situ STM and SMC of F_4TCNQ on Au(111). In order to study the effect of electron withdrawing groups on the molecule−substrate interaction and the electrical conductance of TCNQ, we introduced fluorine atoms to the TCNQ molecule and recorded STM images of the F_4TCNQ adlayers on Au(111). The STM image (Figure 3a) shows the formation of an ordered layer of F_4TCNQ on Au(111). The lack of a herringbone structure underneath the molecular layer is indicative of a stronger molecule−surface interaction relative to what was observed for TCNQ. With four electronegative fluorine atoms, F_4TCNQ is a stronger electron acceptor than TCNQ, and it affects the charge density on the Au(111) surface, possibly through charge transfer between the molecule and the surface as evidenced by the lifting of the reconstruction observed in STM images and CV (Figures S1 and S5) while TCNQ does not seem to affect the Au(111) surface.[42] Moreover, the dominant intermolecular interaction in the TCNQ adlayer, the hydrogen bonding between TCNQ molecules, is hindered by replacing the hydrogen atoms in TCNQ with fluorine atoms in F_4TCNQ. This suggests that the interaction between the F_4TCNQ molecules and the Au(111) surface is the dominant force in the formation of the ordered structure on the surface, rather than intermolecular interactions. On the basis of the STM observations and the cross-section analysis, each rectangular shaped F_4TCNQ molecule was determined to be adsorbed on Au(111) in a flat-lying orientation (Figure 3a) forming a unit cell that contains one F_4TCNQ molecule. Further details are provided in the Supporting Information (Figure S4). Previous STM studies under UHV report images that show the formation of F_4TCNQ networks on Au(111) and Cu(100) surfaces similar to those observed in this study.[41−43] To the best of our knowledge, this is the first STM report of ordered structure formation of F_4TCNQ in an electrochemical environment.

In order to study the effect of an electron withdrawing group on charge transport through benzene derivatives and to validate our hypothesis that such molecules can exhibit denticity dependent conductance, we performed a series of SMC measurements on the negatively charged Au(111) in the

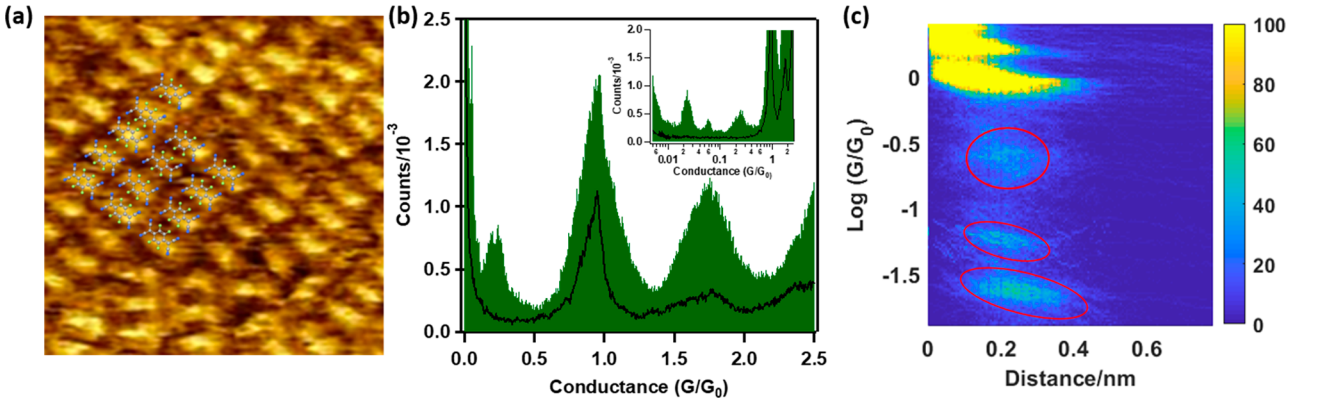

Figure 3. (a) STM image of F_4TCNQ/0.05 M H_2SO_4 on Au(111) at V_S = 0.05 V_{SCE}, V_{bias} = 0.03 V, and I_t = 0.1 nA, scan area 10 × 10 nm^2. (b) Conductance histograms for F_4TCNQ recorded in 0.05 M H_2SO_4 at V_S = 0.05 V_{SCE} (green, generated using 4429 current-distance curves) and V_S = 0.7 V_{SCE} (black line, generated using 1388 current-distance curves) at V_{bias} = 0.05 V. The inset is the log binned conductance histograms recorded at V_S = 0.05 V_{SCE} (green, generated using 4429 current-distance curves) and V_S = 0.7 V_{SCE} (black line, generated using 1388 current-distance curves) at V_{bias} = 0.05 V. (c) 2D histogram generated from data recorded at V_S = 0.05 V_{SCE}. All histograms are generated without data selection.

https://dx.doi.org/10.1021/acs.jpcc.9b10566
J. Phys. Chem. C 2020, 124, 9460−9469

presence of F_4TCNQ molecules. The 1D and 2D conductance histograms constructed from more than 3000 current−distance curves show three well-defined peaks in the linear histogram at 0.24, 1.00, and 1.8 G_0 (Figure 3b,c). The molecular conductance peak appearing at 0.24 G_0 implies the direct coupling of the π-system of the central ring of F_4TCNQ with the gold surface.[22−24,47−49] The 1.00 and 1.8 G_0 features are assigned to the conductance of one and two transmission channels of Au−Au junctions, respectively. These observations support our general hypothesis that flat oriented molecules allow for Au−molecule−Au junction formation and facilitate charge transport measurements perpendicular to the molecular plane.[24]

The TCNQ conductance histogram showed two low conductance (<0.1 G_0) peaks which were assigned to different configurations of the molecule in the junction due to the molecule being lifted up by the tip contacting one or more CN anchoring groups. Closer inspection of the 1D histogram of F_4TCNQ shows two peaks at 0.02 and 0.05 G_0 (Figure. 3b, inset), close to the values observed in the TCNQ conductance histogram (Figure 1b, inset). This is reasonable as the two molecules have similar backbones and anchoring groups. A previous study investigated electrical transport through a charge transfer complex including F_4TCNQ as an electron acceptor.[45] The 2D conductance histogram of F_4TCNQ was reported as a control experiment in air without any solvent (not in an electrochemical environment as in this study) and shows the presence of two different plateaus. These data were not discussed. While one of the plateaus is consistent with the conductance we assigned to the monodentate-bidentate configuration in our study, no high conductance plateau was observed, most likely because the molecule was not deposited in an orientation-controlled manner. The histogram constructed from current−distance curves measured at the positively charged gold surface does not show well-defined peaks in the high current range except for the one and two gold atomic conductances as was the case for TCNQ (Figure 3b, black line). The lack of high conductance peaks is likely due to the absence of an ordered adsorbate structure, suggesting a random and possibly nonplanar orientation of molecules on the positively charged surface as observed in the STM images (Figure S5).

To confirm that the observed conductance values are fingerprints of molecules in the junction, we performed STM-BJ control experiments in blank 0.05 M H_2SO_4 on the negatively charged Au(111) in the high current region where the high conductance peak is observed in the presence of TCNQ/F_4TCNQ, and in the low current region where low conductance values were observed. The resulting histograms showed the absence of high/low conductance features, demonstrating that the observed conductance values are associated with TCNQ/F_4TCNQ molecules (Figure S11a,b). Furthermore, we ran a series of STM-BJ measurement for both TCNQ and F_4TCNQ with different biases while the surface potential was kept constant. The resulting histograms show that the current maxima move to higher values as the bias increases, indicating a bias independence of the molecular conductance (Figures S12 and S13).

DFT Calculations. To provide further insight into the conductance of the two molecules, DFT calculations and NEGF methods were used to study charge transport in TCNQ and F_4TCNQ from first principles. The results for F_4TCNQ are presented in detail, while those for TCNQ are included in the Supporting Information (SI). The differences between the results for the two molecules will be discussed below. Multiple peaks found in the SMC data suggest there is more than one distinct way in which a molecule can bridge the gold−gold junction. It is assumed that the more energetically favorable the molecular junction is, the more likely it is to form and be measured in the SMC experiment. Factors such as the shape of the electrodes, the distance between electrodes, and the orientation of the molecule will affect the stability (energy) and ultimately the transmission through the molecule. Sampling all of these possibilities computationally would be an intractable task and is not attempted. The approach taken here is to look at a small but intuitively distinct set of configurations and determine the different possible regimes of transmission associated with TCNQ and F_4TCNQ.

The first feature used to distinguish between junction configurations is the direction of the transport relative to the π-system of the molecule. The second is how many −CN anchoring groups are coupled to each electrode (denticity). This approach allows us to focus on the four molecular orientations shown in Figure 4. Different variations of each orientation were also studied (included in the SI), in some cases giving rise to a range of conductance values for a given denticity, though this change in conductance is much smaller than the change found from varying the denticity.

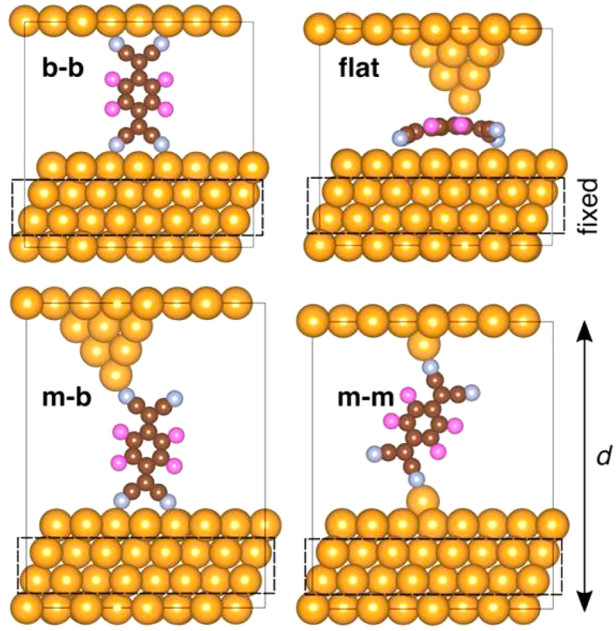

Figure 4. F_4TCNQ geometries for which transmission is calculated. Two gold layers are fixed (inside dashed box) during optimization while other gold layers, apexes, and molecules are free to move. Left, top: bidentate−bidentate (b−b) anchoring. Left, bottom: monodentate−bidentate (m−b) anchoring. Right, top: adsorbed molecule (flat) with apex allowing for transport directly through (perpendicular to) the π-system. Right, bottom: monodentate−monodentate (m−m) anchoring.

In three of the geometries, the molecule is oriented along its longest axis between the electrodes with different denticities, i.e., monodentate (m) or bidentate (b). For example, the bidentate−bidentate (b−b) orientation in Figure 4 (top, left) is named as such since two −CN groups are attached to the top electrode and two −CN groups are attached to the bottom

https://dx.doi.org/10.1021/acs.jpcc.9b10566
J. Phys. Chem. C 2020, 124, 9460−9469

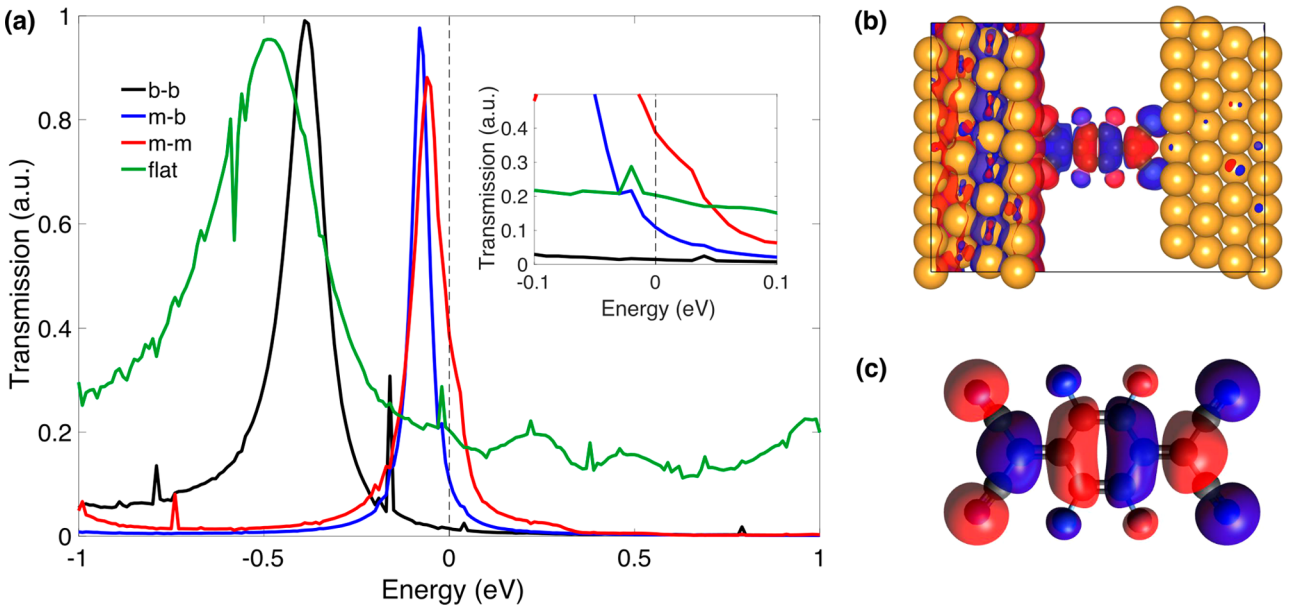

Figure 5. (a) Calculated transmission spectra for F_4TCNQ in the bidentate−bidentate (black), monodentate−bidentate (blue), monodentate−monodentate (red), and flat (green) configurations. The spectrum shown for the flat configuration is for the Au tip aligned above a carbon atom in the benzene ring. Inset: Transmission spectra in the vicinity of the Fermi energy (Fermi energy at 0 eV). (b) Scattering state wave function of the bidentate−bidentate geometry corresponding to the peak in the transmission spectra at −0.4 eV. (c) The LUMO of an isolated F_4TCNQ molecule obtained with hybrid DFT calculation.

electrode. The b−b, m−b, and m−m orientations are assumed to have transport along the extended π-system of the molecule. In the flat geometry (top, right of Figure 4), the molecule is adsorbed flat on the Au(111) surface and assumed to have transport in the direction perpendicular to the π-system.

The transmission is sensitive to the coupling of the molecule to the electrodes, which is largely governed by the Au−N distance in the b−b, m−b, and m−m orientations and the Au−C distance in the flat orientation. To find the most energetically favorable coupling for each orientation, DFT calculations were performed using VASP[65] at different electrode separations. The Perdew−Burke−Ernzerhof (PBE)[66] form of the generalized gradient approximation was employed as the exchange-correlation functional along with the D3 van der Waals correction.[67] Since VASP uses periodic boundary conditions, the electrode separation was controlled by varying the length of the unit cell vector perpendicular to the gold surface. A calculation of the energy is performed at a fixed cell length and allows all atoms to move except those in the two fixed gold layers (see Figure 4). Next, the top electrode is moved 0.1 Å by changing the cell length, *d*. This process is performed sequentially to determine the minimum energy cell length/molecule−electrode coupling. Further details on the ground state DFT calculations performed are provided in the SI. Transmission coefficients were calculated at zero bias using the Nanodcal code.[68,69] The low bias conductance, defined as the value of the transmission function at the Fermi energy, is presented. The conductance of the minimum energy structure, found via ground state DFT calculations, is reported as the conductance for each of the four orientations.

The transmission spectra for F_4TCNQ (Figure 5a) show that the b−b and m−b geometries give conductances of 0.01−0.03 (depending on electrode model) and ∼0.1 G_0, respectively, while the flat geometry gives a higher conductance which depends on where the Au tip aligns above the molecule. Above a central benzene C−C bond, the conductance is ∼0.1 G_0, and above a benzene C atom, it is ∼0.2 G_0 (Figure S17). In the case of m−b, the electrode shape options are also limited (compared to b−b) by the need to maximize the distance between the unanchored −CN so as to have no coupling between it and the electrode surface, requiring a large apex on one electrode.

The F_4TCNQ results are in good agreement with the experimental results discussed above and allow us to assign specific geometries to the different measured conductances. As expected, the flat geometry gives a higher conductance compared to b−b and m−b due to the direct coupling between the metal surface and the π-system of the benzene ring. Somewhat unanticipated, the calculations predict that conductance increases as the denticity decreases. This leads to the m−m geometry giving a relatively high conductance of ∼0.4 G_0, larger than that of the flat orientation. Neither manual screening of the STM-BJ data nor the 1D conductance histogram revealed a separate feature near 0.4 G_0. CN anchored m−m junctions have been observed previously[51] where an m−m junction is the only viable configuration across a wide range of electrode separations. In the case of F_4TCNQ, there are two other junctions, the b−b and m−b, that are geometrically similar to the m−m junction with which the m−m junction must compete. One could argue that the junction will remain b−b or m−b anchored until the molecule is "forced" into a m−m anchored junction, e.g., when the electrodes are maximally separated, making a long-lived m−m junction less likely to form.

The transmission spectra for b−b, m−b, and m−m junctions (Figure 5a) are similar in character. The low conductance in the b−b geometry is a clear result of the larger misalignment of the frontier orbital energy (the peak at −0.4 eV) with the Fermi level (0 eV) compared to those of the m−b and m−m geometries. For geometries with transport along the π-system, it appears that decreasing the denticity shifts the frontier orbital closer to the Fermi energy, increasing the transmission.

https://dx.doi.org/10.1021/acs.jpcc.9b10566
J. Phys. Chem. C 2020, 124, 9460−9469

This is the origin of the inverse correlation between denticity and conductance observed for F_4TCNQ.

Scattering state calculations were performed on the four systems to determine which molecular orbitals contribute to the transmission peaks. For example, Figure 5b shows the scattering state wave function for the b−b system (black) at −0.4 eV in the transmission spectrum. The MO wave functions of the isolated molecule (calculated with hybrid DFT [B3LYP[70]/6-311G(d,p)], though other methods yield similar results) reveal that this closely resembles the lowest unoccupied molecular orbital (LUMO) (Figure 5c), meaning that this MO is the primary channel for transport through the junction. The same analysis provided in the Supporting Information shows that the LUMO is also mediating the transport in TCNQ. As strong electron acceptors, it is reasonable for the LUMO of TCNQ and F_4TCNQ to drop below the Fermi energy when interacting with the Au electrodes as the molecules receive electrons and their LUMOs become occupied. This analysis explains how higher conductance in these molecules is caused by weaker coupling to the electrodes since it raises the energy of the LUMO level, bringing it closer to E_F.

While STM-BJ histograms found that the conductance values do not vary significantly between the two molecules, calculations with TCNQ showed higher conductance compared to F_4TCNQ in the three systems with transport parallel to the π-system. Experimental and theoretical conductance values of F_4TCNQ and TCNQ are provided in Table 1. The TCNQ b−b, m−b, and m−m orientations give

Table 1. Summary of Experimental and Calculated Conductance Values of TCNQ and F_4TCNQ[a]

molecule	configuration	conductance (exp) (G_0)	conductance (theory) (G_0)
TCNQ	quasi-flat	0.220 ± 0.005	0.2
	mono−mono	N/A	0.6
	mono−bi	0.055 ± 0.010	0.2
	bi−bi	0.024 ± 0.007	0.06−0.09
F_4TCNQ	quasi-flat	0.24 ± 0.01	0.1/0.2
	mono−mono	N/A	0.4
	mono−bi	0.051 ± 0.003	0.1
	bi−bi	0.022 ± 0.002	0.01−0.03

[a]Error bars are the standard deviation of the peak position for repeated measurements (typically four times).

conductances of 0.06−0.09 (see Figures S19 and S20), ∼0.2, and ∼0.6 G_0, respectively. As found for F_4TCNQ, the conductance increases as the number of −CN anchors decreases (see SI for transmission spectra). The TCNQ flat geometry gives a conductance of ∼0.2 G_0 when the Au tip aligns above the same benzene C atom as in F_4TCNQ, which gave the same conductance. Unlike for F_4TCNQ, the conductance through the benzene C−C bond aligned tip does not change significantly for TCNQ, remaining at ∼0.2 G_0. An explanation for this difference may be a combination of several factors including frontier orbital alignment, registry of the molecule on the Au surface, as well as the strength of interaction with the surface, i.e., coupling.

The reason for the larger conductance in TCNQ than F_4TCNQ is somewhat clearer for b−b, m−b, and m−m. Since the LUMO shifts downward in energy upon replacing the four hydrogen atoms with fluorine atoms (going from TCNQ to F_4TCNQ), the LUMO of TCNQ naturally aligns closer to the Fermi energy compared to that of F_4TCNQ. This leads to an overall increase in the TCNQ conductance values. This inherent energy shift in the orbitals is apparent in the calculations but not in the experiments where the same conductance peaks appear in the histograms for both molecules. One possibility is that the different interactions between molecules in the monolayer alter the energy alignment, since there is intermolecular hydrogen bonding in TCNQ but not in F_4TCNQ. Another possibility is that one molecule interacts more readily with the solvent than the other, again altering the energy alignment. Exploring these effects would provide insight into the discrepancy between theory and experiment but was beyond the scope of the present work and should be investigated in the future. Despite the differences from F_4TCNQ, the TCNQ b−b geometry still produces a low conductance value, and the flat geometry conductance is similar to that of F_4TCNQ, both in agreement with the experimental results (Table 1). In summary, the theoretical model produces multiple conductance values within or near the range of the experimental histogram peaks (0.02−0.20 G_0) and provides insight into how variation of the molecular geometry in the junction can lead to multiple distinct conductance values.

CONCLUSIONS

In the present study, we have fabricated single TCNQ and F_4TCNQ molecule junctions using the STM-BJ method to investigate the orientation and denticity dependence of the electrical transport properties of these molecules. The potential applied to the gold surface enables the formation of an ordered molecular network on the electrode and control of the geometry of the target molecules in the junction. The single molecule conductance measurement results show that the quasi-flat oriented TCNQ and F_4TCNQ molecules on the negatively charged Au(111), identified by STM imaging, exhibit high conductance of ∼0.220 G_0 ± 0.005 and 0.24 G_0 ± 0.01, respectively, due to the direct π interaction of the benzene ring with the metal electrode. Furthermore, the appearance of the first plateau in current−distance traces (∼0.2 G_0) is expected to be associated with the initial quasi-flat configuration, further supporting the assignment of high conductance (0.2 G_0) to the conductance through the π-system of the central ring. However, the proposed model is a simplified picture of a molecule in the junction and does not consider the uncertainty in the local electrode geometry. In addition to the high conductance, two lower values of 0.02 and 0.05 G_0 are detected, whereas on the positively charged electrode no high conductance states are detected, possibly due to the lack of ordered structure as revealed by STM images.

Several low conductance values were observed at positively charged surfaces in the low current range that could be assigned to different vertical orientations of the molecule in the junction, as supported by calculations. MPVC analysis of the data revealed a broad range of molecular junction behaviors, presumably originating from different molecular configurations in the electrode junction and dynamic switching.

Computational modeling of transport through single molecules of F_4TCNQ and TCNQ shows a clear dependence of the conductance on molecular denticity and molecular orientation in the junction. For a small number of carefully selected model geometries, the theoretical calculation

https://dx.doi.org/10.1021/acs.jpcc.9b10566
J. Phys. Chem. C 2020, 124, 9460−9469

reproduces experimentally observed conductance values well, thereby supporting our structural interpretation of the data. Both molecules have a calculated conductance of ~0.2 G_0 when transport is perpendicular to the π-system of the molecule (lying quasi-flat), which agrees well with the experimental histogram peak at ~0.2 G_0, though slightly different geometries yield lower calculated conductances. For transport along the molecular backbone, the calculated conductance reaches 0.6/0.4 G_0 for TCNQ/F_4TCNQ, for those systems with the lowest denticity. Effects not accounted for by the calculations, such as intermolecular interactions within the monolayer and the presence of a solvent, are possible reasons why the influence of orbital alignment is not seen in the experiment. It is proposed that the low experimental conductance value (0.02 G_0) is due to a bidentate−bidentate linked junction, the peak at 0.05 G_0 to a monodentate-bidentate linked junction, and the high conductance value (0.2 G_0) to a quasi-flat geometry.

Our findings provide insight into the fundamentally important process of charge transport at a molecule−metal contact. The observed experimental and theoretical results reveal that, depending on the denticity, molecule−metal hybridization, and energy level alignment, the electrical conductance through a single molecule can be manipulated in a controllable manner. Particularly, our results show that the stronger interaction between the molecule and the metal electrode does not always guarantee the effective electrical coupling and better charge transport. These findings open new perspectives toward designing single-molecule devices and tuning the molecule−metal interface.

■ ASSOCIATED CONTENT

Supporting Information

The Supporting Information is available free of charge at https://pubs.acs.org/doi/10.1021/acs.jpcc.9b10566.

Solution and materials, cyclic voltammetry, *in situ* scanning tunneling microscopy (STM), *in situ* scanning tunneling microscopy-break junction (STM-BJ), MPVC analysis, STM-BJ control experiments, single molecule conductance vs sample potential, and DFT calculations (PDF)

■ AUTHOR INFORMATION

Corresponding Authors

Manuel Smeu − *Department of Physics, Binghamton University, Binghamton, New York 13902, United States;* orcid.org/0000-0001-9548-4623; Email: msmeu@binghamton.edu

Eric Borguet − *Department of Chemistry, Temple University, Philadelphia, Pennsylvania 19122, United States;* orcid.org/0000-0003-0593-952X; Email: eborguet@temple.edu

Authors

Parisa Yasini − *Department of Chemistry, Temple University, Philadelphia, Pennsylvania 19122, United States;* orcid.org/0000-0001-8072-6597

Stuart Shepard − *Department of Physics, Binghamton University, Binghamton, New York 13902, United States*

Tim Albrecht − *School of Chemistry, University of Birmingham, Birmingham, United Kingdom;* orcid.org/0000-0001-6085-3206

Complete contact information is available at: https://pubs.acs.org/10.1021/acs.jpcc.9b10566

Author Contributions

P.Y. and E.B. designed the experiments. P.Y. performed the experiments. P.Y. and E.B. performed analysis of experimental results. S.S. and M.S. performed transport calculations. T.A. performed the MPVC analysis. The manuscript was written through the contributions of all authors. All authors have given approval to the final version of the manuscript

Notes

The authors declare no competing financial interest.

■ ACKNOWLEDGMENTS

This work was supported by funding from National Science Foundation (CHE-1508567). S.S. and M.S. were supported by funding from Binghamton University. NEGF-DFT calculations were performed on the Spiedie HPC cluster at Binghamton University and the Extreme Science and Engineering Discovery Environment (XSEDE, supported by NSF Grant ACI-1053575). T.A. would like to thank the EPSRC (EP/N032977) for support.

■ REFERENCES

(1) Komoto, Y.; Fujii, S.; Nakamura, H.; Tada, T.; Nishino, T.; Kiguchi, M. Resolving metal-molecule interfaces at single-molecule junctions. *Sci. Rep.* **2016**, *6*, 26606.

(2) Joachim, C.; Ratner, M. A. Molecular electronics: Some views on transport junctions and beyond. *Proc. Natl. Acad. Sci. U. S. A.* **2005**, *102*, 8801.

(3) Bi, H.; Palma, C.-A.; Gong, Y.; Hasch, P.; Elbing, M.; Mayor, M.; Reichert, J.; Barth, J. V. Voltage-Driven Conformational Switching with Distinct Raman Signature in a Single-Molecule Junction. *J. Am. Chem. Soc.* **2018**, *140*, 4835−4840.

(4) Bian, B.-A.; Zheng, Y.-P.; Yuan, P.-P.; Liao, B. I. N.; Ding, Y.-Q. First-Principles Study on Photoswitching Behavior in Single Molecule Junction. *Surf. Rev. Lett.* **2018**, *25*, 1850070.

(5) Brooke, R. J.; Szumski, D. S.; Vezzoli, A.; Higgins, S. J.; Nichols, R. J.; Schwarzacher, W. Dual Control of Molecular Conductance through pH and Potential in Single-Molecule Devices. *Nano Lett.* **2018**, *18*, 1317−1322.

(6) Ismael, A. K.; Wang, K.; Vezzoli, A.; Al-Khaykanee, M. K.; Gallagher, H. E.; Grace, I. M.; Lambert, C. J.; Xu, B.; Nichols, R. J.; Higgins, S. J. Side-Group-Mediated Mechanical Conductance Switching in Molecular Junctions. *Angew. Chem., Int. Ed.* **2017**, *56*, 15378−15382.

(7) Li, Y.; Haworth, N. L.; Xiang, L.; Ciampi, S.; Coote, M. L.; Tao, N. Mechanical Stretching-Induced Electron-Transfer Reactions and Conductance Switching in Single Molecules. *J. Am. Chem. Soc.* **2017**, *139*, 14699−14706.

(8) Li, Z.; Smeu, M.; Afsari, S.; Xing, Y.; Ratner, M. A.; Borguet, E. Single-Molecule Sensing of Environmental pH—an STM Break Junction and NEGF-DFT Approach. *Angew. Chem., Int. Ed.* **2014**, *53*, 1098−1102.

(9) Gaudenzi, R.; de Bruijckere, J.; Reta, D.; Moreira, I. d. P. R.; Rovira, C.; Veciana, J.; van der Zant, H. S. J.; Burzurí, E. Redox-Induced Gating of the Exchange Interactions in a Single Organic Diradical. *ACS Nano* **2017**, *11*, 5879−5883.

(10) Li, Z.; Li, H.; Chen, S.; Froehlich, T.; Yi, C.; Schönenberger, C.; Calame, M.; Decurtins, S.; Liu, S.-X.; Borguet, E. Regulating a Benzodifuran Single Molecule Redox Switch via Electrochemical Gating and Optimization of Molecule/Electrode Coupling. *J. Am. Chem. Soc.* **2014**, *136*, 8867−8870.

(11) Li, Z.; Smeu, M.; Rives, A.; Maraval, V.; Chauvin, R.; Ratner, M. A.; Borguet, E. Towards graphyne molecular electronics. *Nat. Commun.* **2015**, *6*, 6321.

(12) Albrecht, T.; Guckian, A.; Ulstrup, J.; Vos, J. G.; et al. Transistor effects and in situ STM of redox molecules at room temperature. *IEEE Trans. Nanotechnol.* **2005**, *4*, 430−434.

(13) Haiss, W.; Albrecht, T.; van Zalinge, H.; Higgins, S. J.; Bethell, D.; Hobenreich, H.; Schiffrin, D. J.; Nichols, R. J.; Kuznetsov, A. M.; Zhang, J.; et al. Single-molecule conductance of redox molecules in electrochemical scanning tunneling microscopy. *J. Phys. Chem. B* **2007**, *111*, 6703−6712.
(14) Albrecht, T.; Mertens, S. F. L.; Ulstrup, J. Intrinsic multistate switching of gold clusters through electrochemical gating. *J. Am. Chem. Soc.* **2007**, *129*, 9162−9167.
(15) Albrecht, T.; Moth-Poulsen, K.; Christensen, J. B.; Hjelm, J.; Bjornholm, T.; Ulstrup, J. Scanning tunneling spectroscopy in an ionic liquid. *J. Am. Chem. Soc.* **2006**, *128*, 6574−6575.
(16) Hosseini, S.; Madden, C.; Hihath, J.; Guo, S.; Zang, L.; Li, Z. Single-Molecule Charge Transport and Electrochemical Gating in Redox-Active Perylene Diimide Junctions. *J. Phys. Chem. C* **2016**, *120*, 22646−22654.
(17) Huang, C. C.; Rudnev, A. V.; Hong, W. J.; Wandlowski, T. Break junction under electrochemical gating: testbed for single-molecule electronics. *Chem. Soc. Rev.* **2015**, *44*, 889−901.
(18) Baghernejad, M.; Zhao, X.; Baruël Ørnsø, K.; Füeg, M.; Moreno-García, P.; Rudnev, A. V.; Kaliginedi, V.; Vesztergom, S.; Huang, C.; Hong, W.; et al. Electrochemical Control of Single-Molecule Conductance by Fermi-Level Tuning and Conjugation Switching. *J. Am. Chem. Soc.* **2014**, *136*, 17922−17925.
(19) Aragones, A.; Darwish, N.; Saletra, W.; Perez-Garcia, L.; Sanz, F.; Puigmarti-Luis, J.; Amabilino, D.; Diez-Perez, I. Highly Conductive Single-Molecule Wires with Controlled Orientation by Coordination of Metalloporphyrins. *Nano Lett.* **2014**, *14*, 4751−4756.
(20) Li, Z. H.; Smeu, M.; Park, T. H.; Rawson, J.; Xing, Y. J.; Therien, M. J.; Ratner, M. A.; Borguet, E. Hapticity-Dependent Charge Transport through Carbodithioate-Terminated [5,15-Bis-(phenylethynyl)porphinato]zinc(II) Complexes in Metal-Molecule-Metal Junctions. *Nano Lett.* **2014**, *14*, 5493−5499.
(21) Zhang, J. D.; Demetriou, A.; Welinder, A. C.; Albrecht, T.; Nichols, R. J.; Ulstrup, J. Potential-induced structural transitions of DL-homocysteine monolayers on Au(111) electrode surfaces. *Chem. Phys.* **2005**, *319*, 210−221.
(22) Yasini, P.; Afsari, S.; Peng, H. W.; Pikma, P.; Perdew, J. P.; Borguet, E. Potential-Induced High-Conductance Transport Pathways through Single-Molecule Junctions. *J. Am. Chem. Soc.* **2019**, *141*, 10109−10116.
(23) Afsari, S.; Yasini, P.; Peng, H. W.; Perdew, J. P.; Borguet, E. Anisotropic Conductivity at the Single-Molecule Scale. *Angew. Chem., Int. Ed.* **2019**, *58*, 14275−14280.
(24) Afsari, S.; Li, Z.; Borguet, E. Orientation-Controlled Single-Molecule Junctions. *Angew. Chem., Int. Ed.* **2014**, *53*, 9771−9774.
(25) Hoshyargar, F.; O'Mullane, A. P. Tetrathiafulvalene−7,7,8,8-Tetracyanoquinodimethane and Tetrathiafulvalene−2,3,5,6-Tetrafluoro-7,7,8,8-tetracyanoquinodimethane Organic Charge-Transfer Complexes: Reusable Catalysts for Electron-Transfer Reactions. *ChemCatChem* **2016**, *8*, 2335−2339.
(26) Hu, P.; Li, H.; Li, Y.; Jiang, H.; Kloc, C. Single-crystal growth, structures, charge transfer and transport properties of anthracene-F4TCNQ and tetracene-F4TCNQ charge-transfer compounds. *CrystEngComm* **2017**, *19*, 618−624.
(27) Hashimoto, S.; Yabushita, A.; Iwakura, I. Real-time observation of interfragment vibration and charge transfer within the TCNQF4 dimer. *Chem. Phys.* **2017**, *493*, 56−60.
(28) Taniguchi, K.; Shito, N.; Fukunaga, H.; Miyasaka, H. Charge-transfer Layered Assembly of a trans-Heteroleptic Paddlewheel-type Diruthenium(II, II) Complex with a TCNQ Derivative: Electrochemical Tuning of the Magnetism. *Chem. Lett.* **2018**, *47*, 664−667.
(29) Torrente, I. F.; Franke, K. J.; Pascual, J. I. Structure and Electronic Configuration of Tetracyanoquinodimethane Layers on a Au(111) Surface. *Int. J. Mass Spectrom.* **2008**, *277*, 269−273.
(30) Le, T. H.; Nafady, A.; Qu, X.; Bond, A. M.; Martin, L. L. Redox and Acid−Base Chemistry of 7,7,8,8-Tetracyanoquinodimethane, 7,7,8,8-Tetracyanoquinodimethane Radical Anion, 7,7,8,8-Tetracyanoquinodimethane Dianion, and Dihydro-7,7,8,8-Tetracyanoquinodimethane in Acetonitrile. *Anal. Chem.* **2012**, *84*, 2343−2350.
(31) Romaner, L.; Heimel, G.; Brédas, J.-L.; Gerlach, A.; Schreiber, F.; Johnson, R. L.; Zegenhagen, J.; Duhm, S.; Koch, N.; Zojer, E. Impact of Bidirectional Charge Transfer and Molecular Distortions on the Electronic Structure of a Metal-Organic Interface. *Phys. Rev. Lett.* **2007**, *99*, 256801.
(32) Park, C.; Rojas, G.; Jeon, S.; Kelly, S.; Smith, S.; Sumpter, B.; Yoon, M.; Maksymovych, P. Weak competing interactions control assembly of strongly bonded TCNQ ionic acceptor molecules on silver surfaces. *Phys. Rev. B: Condens. Matter Mater. Phys.* **2014**, *90*, 125432.
(33) Rodríguez-Fernández, J.; Robledo, M.; Lauwaet, K.; Martín-Jiménez, A.; Cirera, B.; Calleja, F.; Díaz-Tendero, S.; Alcamí, M.; Floreano, L.; Domínguez-Rivera, M.; et al. Tuning Intermolecular Charge Transfer in Donor−Acceptor Two-Dimensional Crystals on Metal Surfaces. *J. Phys. Chem. C* **2017**, *121*, 23505−23510.
(34) Le, T. H.; Lu, J.; Bond, A. M.; Martin, L. L. Identification of $TCNQF_4$ Redox Levels using Spectroscopic and Electrochemical Fingerprints ($TCNQF_4$=2,3,5,6-tetrafluoro-7,7,8,8-tetracyanoquinodimethane). *Inorg. Chim. Acta* **2013**, *395*, 252−254.
(35) Xiao, K.; Rondinone, A. J.; Puretzky, A. A.; Ivanov, I. N.; Retterer, S. T.; Geohegan, D. B. Growth, Patterning, and One-Dimensional Electron -Transport Properties of Self-Assembled Ag-TCNQF4 Organic Nanowires. *Chem. Mater.* **2009**, *21*, 4275−4281.
(36) Jeon, S.; Doak, P.; Sumpter, B.; Ganesh, P.; Maksymovych, P. Thermodynamic Control of Two-Dimensional Molecular Ionic Nanostructures on Metal Surfaces. *ACS Nano* **2016**, *10*, 7821−7829.
(37) Blowey, P. J.; Haags, A.; Rochford, L. A.; Felter, J.; Warr, D. A.; Duncan, D. A.; Lee, T.-L.; Costantini, G.; Kumpf, C.; Woodruff, D. P. Characterization of growth and structure of TCNQ phases on Ag(111). *Phys. Rev. Materials* **2019**, *3*, 116001.
(38) Stradi, D.; Borca, B.; Barja, S.; Garnica, M.; Díaz, C.; Rodríguez-García, J. M.; Alcamí, M.; Vázquez de Parga, A. L.; Miranda, R.; Martín, F. Understanding the self-assembly of TCNQ on Cu(111): a combined study based on scanning tunnelling microscopy experiments and density functional theory simulations. *RSC Adv.* **2016**, *6*, 15071.
(39) Yan, H.; Li, S.; Yan, C.; Chen, Q.; Wan, L. Adsorption of TTF, TCNQ and TTF-TCNQ on Au(111): An in situ EC-STM study. *Sci. China, Ser. B: Chem.* **2009**, *52*, 559−565.
(40) Wan, L.; Kingo, I. Adlayer Structure of TCNQ Molecules on Cu(111): An In Situ STM Study. *Chin. Sci. Bull.* **2001**, *46*, 377−380.
(41) Jackel, F.; Perera, U.; Iancu, V.; Braun, K.; Koch, N.; Rabe, J.; Hla, S. Investigating molecular charge transfer complexes with a low temperature scanning tunneling microscope. *Phys. Rev. Lett.* **2008**, *100*, 24558.
(42) Faraggi, M.; Jiang, N.; Gonzalez-Lakunza, N.; Langner, A.; Stepanow, S.; Kern, K.; Arnau, A. Bonding and Charge Transfer in Metal-Organic Coordination Networks on Au(111) with Strong Acceptor Molecules. *J. Phys. Chem. C* **2012**, *116*, 24558−24565.
(43) Katayama, T.; Mukai, K.; Yoshimoto, S.; Yoshinobu, J. Reactive rearrangements of step atoms by adsorption and asymmetric electronic states of tetrafluoro-tetracyanoquinodimethane on Cu(100). *Phys. Rev. B: Condens. Matter Mater. Phys.* **2011**, *83*, 153403.
(44) Wickenburg, S.; Lu, J.; Lischner, J.; Tsai, H.; Omrani, A.; Riss, A.; Karrasch, C.; Bradley, A.; Jung, H.; Khajeh, R.; et al. Tuning Charge and Correlation Effects for a Single Molecule on a Graphene Device. *Nat. Commun.* **2016**, *7*, 13553.
(45) García, R.; Herranz, M. Á.; Leary, E.; González, M. T.; Bollinger, G. R.; Bürkle, M.; Zotti, L. A.; Asai, Y.; Pauly, F.; Cuevas, J. C.; et al. Single-molecule conductance of a chemically modified, π-extended tetrathiafulvalene and its charge-transfer complex with F4TCNQ. *Beilstein J. Org. Chem.* **2015**, *11*, 1068−1078.
(46) He, Y.; Ye, T.; Borguet, E. The role of hydrophobic chains in self-assembly at electrified interfaces: Observation of potential-induced transformations of two-dimensional crystals of hexadecane by in-situ scanning tunneling microscopy. *J. Phys. Chem. B* **2002**, *106*, 11264−11271.

https://dx.doi.org/10.1021/acs.jpcc.9b10566
J. Phys. Chem. C 2020, 124, 9460−9469

(47) Komoto, Y.; Fujii, S.; Nishino, T.; Kiguchi, M. High Electronic Couplings of Single Mesitylene Molecular Junctions. *Beilstein J. Nanotechnol.* **2015**, *6*, 2431−2437.
(48) Kiguchi, M.; Kaneko, S. Electron Transport through Single π-Conjugated Molecules Bridging between Metal Electrodes. *ChemPhysChem* **2012**, *13*, 1116−1126.
(49) Kiguchi, M.; Murakoshi, K. Highly Conductive Single Molecular Junctions by Direct Binding of π-Conjugated Molecule to Metal Electrodes. *Thin Solid Films* **2009**, *518*, 466−469.
(50) Iwane, M.; Fujii, S.; Nishino, T.; Kiguchi, M. Single Tripyridyl−Triazine Molecular Junction with Multiple Binding Sites. *J. Phys. Chem. C* **2016**, *120*, 8936−8940.
(51) Mishchenko, A.; Zotti, L. A.; Vonlanthen, D.; Bürkle, M.; Pauly, F.; Cuevas, J. C.; Mayor, M.; Wandlowski, T. Single-Molecule Junctions Based on Nitrile-Terminated Biphenyls: A Promising New Anchoring Group. *J. Am. Chem. Soc.* **2011**, *133*, 184−187.
(52) Kaliginedi, V.; Rudnev, A. V.; Moreno-Garcia, P.; Baghernejad, M.; Huang, C.; Hong, W.; Wandlowski, T. Promising anchoring groups for single-molecule conductance measurements. *Phys. Chem. Chem. Phys.* **2014**, *16*, 23529−23539.
(53) Li, Z.; Smeu, M.; Ratner, M. A.; Borguet, E. Effect of Anchoring Groups on Single Molecule Charge Transport through Porphyrins. *J. Phys. Chem. C* **2013**, *117*, 14890−14898.
(54) Moreno-García, P.; Gulcur, M.; Manrique, D. Z.; Pope, T.; Hong, W.; Kaliginedi, V.; Huang, C.; Batsanov, A. S.; Bryce, M. R.; Lambert, C.; et al. Single-Molecule Conductance of Functionalized Oligoynes: Length Dependence and Junction Evolution. *J. Am. Chem. Soc.* **2013**, *135*, 12228−12240.
(55) Kitaguchi, Y.; Habuka, S.; Okuyama, H.; Hatta, S.; Aruga, T.; Frederiksen, T.; Paulsson, M.; Ueba, H. Controlling single-molecule junction conductance by molecular interactions. *Sci. Rep.* **2015**, *5*, 11796.
(56) Park, Y. S.; Widawsky, J. R.; Kamenetska, M.; Steigerwald, M. L.; Hybertsen, M. S.; Nuckolls, C.; Venkataraman, L. Frustrated Rotations in Single-Molecule Junctions. *J. Am. Chem. Soc.* **2009**, *131*, 10820−10821.
(57) Chen, F.; Li, X.; Hihath, J.; Huang, Z.; Tao, N. Effect of anchoring groups on single-molecule conductance: comparative study of thiol-, amine-, and carboxylic-acid-terminated molecules. *J. Am. Chem. Soc.* **2006**, *128*, 15874−81.
(58) Kim, Y.; Lenert, A.; Meyhofer, E.; Reddy, P. Temperature Dependence of Thermopower in Molecular Junctions. *Appl. Phys. Lett.* **2016**, *109*, 033102.
(59) Kiguchi, M.; Nakamura, H.; Takahashi, Y.; Takahashi, T.; Ohto, T. Effect of Anchoring Group Position on Formation and Conductance of a Single Disubstituted Benzene Molecule Bridging Au Electrodes: Change of Conductive Molecular Orbital and Electron Pathway. *J. Phys. Chem. C* **2010**, *114*, 22254−22261.
(60) Xiao, X.; Xu, B.; Tao, N. Measurement of single molecule conductance: Benzenedithiol and benzenedimethanethiol. *Nano Lett.* **2004**, *4*, 267−271.
(61) Kaneko, S.; Nakamura, Y.; Matsushita, R.; Marques-Gonzalez, S.; Kiguchi, M. Simultaneous measurement of electrical conductance and thermopower of single benzenedithiol molecular junctions. *Appl. Phys. Express* **2015**, *8*, 065201.
(62) Tanimoto, S.; Tsutsui, M.; Yokota, K.; Taniguchi, M. Dipole Effects on the Formation of Molecular Junctions. *Nanoscale Horiz.* **2016**, *1*, 399−406.
(63) Hong, W. J.; Manrique, D. Z.; Moreno-Garcia, P.; Gulcur, M.; Mishchenko, A.; Lambert, C. J.; Bryce, M. R.; Wandlowski, T. Single Molecular Conductance of Tolanes: Experimental and Theoretical Study on the Junction Evolution Dependent on the Anchoring Group. *J. Am. Chem. Soc.* **2012**, *134*, 2292−2304.
(64) Lemmer, M.; Inkpen, M.; Kornysheva, K.; Long, N.; Albrecht, T. Unsupervised vector-based classification of single-molecule charge transport data. *Nat. Commun.* **2016**, *7*, 12922.
(65) Kresse, G.; Furthmuller, J. Efficient Iterative Schemes for Ab Initio Total-Energy Calculations Using a Plane-Wave Basis Set. *Phys. Rev. B: Condens. Matter Mater. Phys.* **1996**, *54*, 11169−11186.
(66) Perdew, J.; Burke, K.; Ernzerhof, M. Generalized gradient approximation made simple. *Phys. Rev. Lett.* **1996**, *77*, 3865−3868.
(67) Grimme, S.; Antony, J.; Ehrlich, S.; Krieg, H. A consistent and accurate ab initio parametrization of density functional dispersion correction (DFT-D) for the 94 elements H-Pu. *J. Chem. Phys.* **2010**, *132*, 154104.
(68) Taylor, J.; Guo, H.; Wang, J. Ab Initio Modeling of Open Systems: Charge Transfer, Electron Conduction, and Molecular Switching of a C-60 Device. *Phys. Rev. B: Condens. Matter Mater. Phys.* **2001**, *63*, 121104.
(69) Taylor, J.; Guo, H.; Wang, J. Ab Initio Modeling of Quantum Transport Properties of Molecular Electronic Devices. *Phys. Rev. B: Condens. Matter Mater. Phys.* **2001**, *63*, 245407.
(70) Becke, A. D.D. Density-Functional Thermochemistry 0.3. The Role of Exact Exchange. *J. Chem. Phys.* **1993**, *98*, 5648−5652.

https://dx.doi.org/10.1021/acs.jpcc.9b10566
J. Phys. Chem. C 2020, 124, 9460−9469